

Article

# Ultra-Fast Heating Treatment Effect on Microstructure, Mechanical Properties and Magnetic Characteristics of Non-Oriented Grain Electrical Steels

Matteo Gaggiotti <sup>1</sup>, Luciano Albini <sup>1</sup>, Giulia Stornelli <sup>2</sup>, Giulia Tiracorrendo <sup>1</sup>, Luca Landi <sup>2</sup> and Andrea Di Schino <sup>2,\*</sup>

<sup>1</sup> RINA Consulting—Centro Sviluppo Materiali SpA, Via Castel Romano 100, 00128 Roma, Italy; matteo.gaggiotti@rina.org (M.G.); luciano.albini@rina.org (L.A.); giulia.tiracorrendo@rina.org (G.T.)

<sup>2</sup> Engineering Department, University of Perugia, Via G. Duranti 93, 06125 Perugia, Italy; giulia.stornelli@unipg.it

\* Correspondence: andrea.dischino@unipg.it

**Abstract:** This paper focuses on the effect of rapid annealing on Non-Grain Oriented Electrical Steel (NGO) in terms of microstructure, mechanical properties, and magnetic properties. The Ultra-Fast Heating (UFH) tests were performed by a transversal induction heater on NGO electrical steel samples (cold rolled down to 0.5 mm), varying the heating power (80 kW and 90 kW) and the speed of the strip through the induction heater. This allowed us to exploit heating rates (HR) in the range of 200–300 °C/s and targeting peak temperature ( $T_{\text{peak}}$ ) up to a maximum of 1250 °C. The comparison between the microstructure as obtained by conventional annealing and the ultra-fast heating process highlights a clear effect in terms of grain size refinement provided by the UFH. In particular, the average grain size as obtained by UFH ranges two/three times lower than by a conventional process. The results show the possibility of applying UFH to NGO steels, targeting mechanical properties such as those obtained by the standard process, combined with the benefits from this innovative heat treatment in terms of green energy and the minimization of CO<sub>2</sub> emissions. Magnetic characterization performed by a single sheet tester (30 × 90 mm) showed that the values of core losses are comparable with conventional NGO grades.

**Keywords:** non-grain oriented electrical steel; ultra-fast heating; conventional annealing; thermal treatment; grain refinement; mechanical properties; magnetic properties

**Citation:** Gaggiotti, M.; Albini, L.; Stornelli, G.; Tiracorrendo, G.; Landi, L.; Di Schino, A. Ultra-Fast Heating Treatment Effect on Microstructure, Mechanical Properties and Magnetic Characteristics of Non-Oriented Grain Electrical Steels.

*Appl. Sci.* **2023**, *13*, 9833.

<https://doi.org/10.3390/app13179833>

Academic Editor: Chen Li

Received: 26 July 2023

Revised: 19 August 2023

Accepted: 29 August 2023

Published: 30 August 2023



**Copyright:** © 2023 by the authors. Licensee MDPI, Basel, Switzerland. This article is an open access article distributed under the terms and conditions of the Creative Commons Attribution (CC BY) license (<https://creativecommons.org/licenses/by/4.0/>).

## 1. Introduction

In recent years, efficiency and sustainability in the energy sector (such as the oil and gas industry, aerospace, and automotive sector—specifically, electric vehicle production) [1–4], along with the demand for a reduction in pollutant emissions, have driven the advancement of materials for such purposes and their manufacturing methodologies.

Electrical steels are the most exploited magnetic material for power application and are classified into two macro-categories: grain-oriented (GO) and non-grain oriented (NGO) electrical steels [5,6]. The first category is used for the generation, transformation, and distribution of electrical energy, while the second one is mostly used in electrical machines such as motors [7–10]. In recent years, due to stringent CO<sub>2</sub> emission targets, the increasing demand of the electric car market led scientists to pay attention to this specific material and to the different industrial routes in its production, including additive manufacturing [11–14]. NGO electrical steels are special grades that are mainly composed of Silicon (Si) and Aluminum (Al), key elements that are able to provide higher values of electrical resistivity [15,16]. Furthermore, there is also an increasing market demand for materials with low magnetic losses to provide higher efficiency motors [17–19]. The standard procedure for non-oriented electrical steels fabrication involves casting, hot

rolling, cold rolling, and final annealing. It is worth mentioning that a wide typology of these materials is produced by steel chemical composition variation (mainly Si and Al content) and acting on process parameters at different processing steps [20–23]. The proper manufacturing route requires a high reduction ratio (higher than 80%) at cold rolling. The final annealing treatment should be realized with the aim of generating a microstructure characterized by a large grain size (about 100  $\mu\text{m}$ ) [24,25]. The thickness reduction [26], combined with a proper recrystallization and grain growth phenomena activated by the subsequent annealing cycle, is necessary to target the proper microstructure and texture [27–32]. Recently, innovative procedures in production have been implemented to satisfy the above requirements [33,34]. In some cases, an additional hot strip annealing before cold rolling is used to achieve commercially higher permeability grades [35,36]. In case of Fe-Si steels with phase transformation, the modification of the hot rolling schedule or hot finishing temperature could improve the magnetization behavior due to the sharper texture components [37–39]. Stöcker et al. [23] investigated the effect of different hot rolling conditions and showed that the highest reduction per pass during hot rolling led to pronounced recrystallization, and consequently, to weaker overall texture and no dominant texture components at the surface. Moreover, after the final annealing, the material exhibited the strongest texture with a strong  $\gamma$ -fiber as an inheritance from the cold rolling step. Since the hot rolled material has undergone different softening mechanisms during hot rolling, it can be assumed that the stored energy after hot rolling (and consequently, after cold rolling) is different, leading to a different amount of strain hardening after cold rolling. Other important observations come from the possibility to modify the chemical composition of NGO steels by reducing undesirable elements such as Sulfur (S), Nitrogen (N), and Oxygen (O) [40,41]. In this context, Schulte et al. [42] showed the effect of Manganese (Mn) on the increase in the electrical resistivity and on loss reduction in Si steels with low S. With this specific condition, the precipitation of undesirable MnS can be prevented and Mn remains in a solid solution. The results showed that Mn addition in a specific range decreases losses and increases permeability, favoring grain growth. Focusing on microstructure and texture, these characteristics are mainly affected by the manufacturing process conditions, and particularly by the cold rolling step and subsequent recrystallization in continuous annealing treatment [20,43–45]. Al and Si also show how to influence NGO steel brittleness [46–48]. This introduces difficulties in the sheet's thickness reduction during cold rolling. For this specific purpose, in order to better homogenize the microstructure and the double stage cold rolling, the annealing of hot rolled coils represents a solution to solve this critical point. The introduction of intermediate annealing treatment allows to obtain further homogenization and reduces the risk of breakage during thickness reduction. Lu et al. [39] demonstrated that a two-step cold rolling process allows to form coarse grain with a strong  $\{110\}\langle 001\rangle$  (Goss) and near Goss texture. In electrical steels,  $\langle 001\rangle$  is the easy magnetization direction, and both Goss and cubic orientation are ideal for magnetic properties [49–50]. After the double-pass cold rolling, the recrystallization during continuous annealing is essential to obtain a strong  $\langle 001\rangle$  direction for superior magnetic properties. The parameters of continuous annealing significantly influence the final microstructure, and the thermal treatment strictly depends on how the hot rolled and cold rolled strips are produced. The aim of continuous annealing in NGO electrical steels at final thickness is to achieve a large grain size in the range of 100–150  $\mu\text{m}$ , a microstructure free of non-metallic inclusions, and a characteristic isotropic magnetic induction on the sheet plane (with optimization of texture and reduction of core losses) [51–53]. However, optimizing magnetic performance is not the only requirement for the class of these materials. For their application in electrical devices, the resistance to mechanical and vibration stresses is a crucial factor. Therefore, the ability to optimize the mechanical performance of NGO steels, without requiring excessive industrial effort, is currently a driving force for developing unconventional manufacturing processes [54,55].

In recent years, the UFH treatment has gained much attention thanks to the possibility to optimize industrial production processes in terms of time, and consequently, productivity [56–59]. The UFH passes through a rapidly alternating magnetic field and allows it to penetrate and generate eddy currents inside the metallic material, thereby providing an electrical heating [60–63]. The UFH exploits an inductor used to heat-treat specific areas faster and with a lower consumption of energy compared with conventional heat treatment, and with several advantages such as shorter processing times, high flexibility, and localized annealing. The main parameters that characterize this rapid annealing are the heating rate (HR) (the temperature variation over time during the heating phase) and the peak temperature (the maximum temperature reached at the end of the heat treatment).

The UFH process has been successfully adopted in stainless steels [64–70], showing results such as those of standard industrial production. This is also confirmed by results collected in the bibliography [57,71] that showed the effect of UFH on mechanical properties in comparison with conventional annealing treatment. A thermal cycle without a holding time, in the case of ferritic stainless steels, resulted in a product that was quite comparable to the industrial standard in a range of heating rates of between 500 and 1000 °C/s. As the holding time increased, the yield strength and tensile strength values remained almost constant, while the total elongation increased. In the case of austenitic stainless steels without any holding time at a peak temperature of 700 °C and a heating rate of 2 and 20 °C/s, the yield strength ( $Y_s$ ) increased up to 870 MPa with an improvement in ductility and elongation. Increasing from 20 to 100 °C/s, the tensile strength and the yield strength did not change too much, but ductility and elongation were improved (elongation showed an extraordinary increase, shifting from 11% to 37%). In terms of mechanical properties, NGO electrical steels can be classified as low-C steels and the effect of UFH can be considered as similar. The evolution of mechanical characteristics was reported in the case of conventional annealing (HR of 10 °C/s) and ultra-fast heating treatment (HR of 500–1000 °C/s) [56]. The results showed that the ultimate tensile strength increased for higher heating rates from a conventional to a UFH annealing. In the same range of heating rates, the yield strength instead decreased while elongation increased.

In this work, the effect of the UFH process on the microstructure, mechanical properties, and magnetic characteristics of NGO steels is studied. The results are discussed in comparison to the properties and characteristics of the same steel grade heat treated through the conventional annealing on a laboratory scale.

## 2. Materials and Methods

The chemical composition of the NGO steel analyzed in this paper is reported in Table 1.

**Table 1.** Steel chemical composition of NGO grade (wt. %; Fe: balance).

| Steel Grade | C (%)  | Si (%) | Al (%) | Mn (%) | N (%)   |
|-------------|--------|--------|--------|--------|---------|
| NGO_050     | 0.0030 | 2.80   | 1.00   | 0.40   | <0.0030 |

The microstructural characteristics (in terms of grain size), and the mechanical and magnetic properties of the samples prepared by the UFH treatment on a laboratory scale are compared with those of the samples obtained by a laboratory annealing simulating an industrial conventional annealing. Moreover, the mechanical properties ( $Y_S$ ,  $R_m$ , and  $A\%$ ) and magnetic properties (core losses and polarization) of the samples obtained by UFH are reported and compared with typical values of the industrial NGO grade.

Specimens  $120 \times 600 \times 0.5 \text{ mm}^3$  in size in the state of cold rolled material with 72% reduction were subjected to UFH annealing laboratory tests. The UFH treatment was carried out by a transversal induction heater. The treatment was performed with specific power (P) conditions (P: 80% and P: 90%) of the maximum allowed power ( $P_{\max} = 100 \text{ kW}$ )

to obtain different HR ranging from 200 up to 270 °C/s, and to reach temperatures in the range between 930 and 1167 °C.

The different investigated experimental conditions are reported in Table 2.

**Table 2.** UFH investigated conditions.

| Specimen Number | P (%) | HR (°C/s) | T <sub>max</sub> (°C) |
|-----------------|-------|-----------|-----------------------|
| 1               | 80    | 213       | 930                   |
| 2               | 80    | 205       | 1014                  |
| 3               | 80    | 206       | 1085                  |
| 4               | 80    | 229       | 1167                  |
| 5               | 90    | 267       | 953                   |
| 6               | 90    | 254       | 1000                  |
| 7               | 90    | 264       | 1038                  |
| 8               | 90    | 265       | 1090                  |

In the induction heating method, the worksheet is considered as a resistor and so a high current is applied to the sheet. The material resistance to the passage of the current produces heat by Joule's effect. The distribution of the current through the sheet is referred to as the "skin effect". The magnitude and depth of the induced current depends on factors such as the dimension of the element that has undergone induction heating, electrical resistivity, magnetic permeability, and frequency of the alternating current (Equation (1)).

$$d = 3160 \sqrt{\frac{\rho}{\mu f}} \quad (1)$$

with:

d = depth of heat penetration

$\rho$  = resistivity of material

$\mu$  = permeability of material

f = frequency of alternating current

As the section size of the material increases, the frequency of the alternating current to be used decreases. All of these considerations are realistic in the case of heat treatment for specimens with significant thicknesses. However, in our specific case, we are considering cold rolled samples with a very low thickness (0.5 mm), suitable for the application of a uniform UFH treatment over the entire section of the sample.

To compare the effect on the microstructural evolution of ultra-fast heating with that obtained by a conventional annealing (CA) cycle, conventional heat treatments were performed on a laboratory scale, with the aim of simulating the industrial continuous annealing process with a HR of about 20–50 °C/s. The heating profile obtained by CA is characterized by a heating stage of 60 s to the peak temperature of 1050 °C and by a 30 s soaking time. Moreover, in order to investigate the real evolution of the microstructure during the CA cycle, the specimens were extracted from the furnace after a soaking time of 10 s, 25 s, 60 s, and 90 s. From the heating profile reported in Figure 1, it appears that after 10 s the sample was extracted after reaching the maximum temperature of 630 °C; instead, after 25 s, the maximum temperature was 965 °C. For the other two soaking times, the samples reached the maximum target temperature of 1050 °C. The CA heat treatments were performed on a tubular furnace with a diameter of 100 mm and a homogeneous thermal zone length of 600 mm; this zone is located in the central region of the furnace and is heated with electric resistance, while the enter zone is cooled through water pipes. All the annealing treatments were carried out in a H<sub>2</sub> atmosphere with a dew point of −40 °C. Before each trial, cleaning operations by N<sub>2</sub> were carried out to guarantee security

requirements. Samples were rapidly positioned inside the central zone (set to the target temperature), heat treated, and then moved to the cooling zone before being extracted.

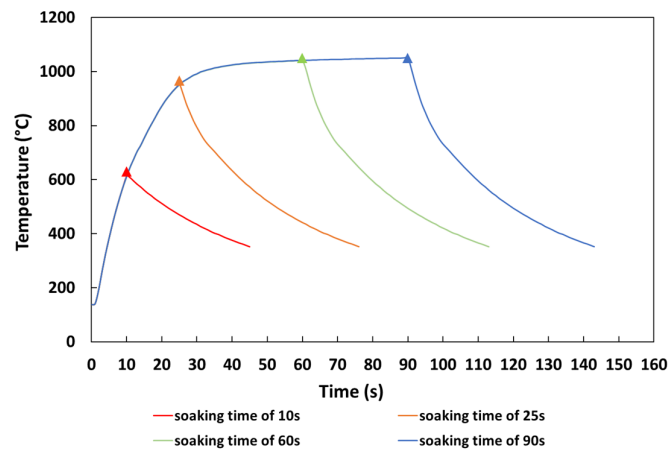


**Figure 1.** Example of conventional annealing treatment cycle as obtained by tubular furnace.

After UFH and CA treatments, specimens were cut, embedded in resin, polished, and then etched in a  $\text{NO}_3 + \text{H}_2\text{O}$  solution. The microstructure was then analyzed using a light microscope (Eclipse LV150 NL, Nikon, Tokyo, Japan) and image analysis was performed using a dedicated software (AlexaSoft, X-Plus, serial number: 6308919690486393, Florence, Italy).

Tensile tests have been performed on ISO-50 specimens and machined parallel to the longitudinal direction, according to the standard ISO 6892-1 through a tensile machine (632.12C-20, produced by MTS) and a maximum load of 100 kN.

Magnetic measurements were performed to characterize the material in terms of anisotropy, core losses, and polarization. Since the maximum width of the coil that can be processed in the UFH Laboratory is 120 mm, it was not possible to perform the magnetic characterization on the Epstein Frame. Therefore, the magnetic measurements were performed by a single sheet tester (SST) on 30 mm × 90 mm samples extracted in both directions, transversal (T—Maximum dimension perpendicular to the rolling direction) and longitudinal (L—maximum dimension, parallel to the rolling direction). The test allowed to obtain the core losses in transversal ( $P_T$ ) and longitudinal ( $P_L$ ) directions with respect to the rolling direction, and consequently, a measurement of anisotropy and specific losses ( $P_S$ ) at a frequency of 50 Hz and a magnetic induction  $B = 1.5$  T. The characteristic values of the magnetic properties obtained through the SST measurements, according to the EN-10106, were the core losses evaluated at two magnetic inductions  $B = 1.0$  T,  $B = 1.5$  T at a frequency of 50 Hz ( $P_{10}$ ,  $P_{15}$ ). The polarization was measured in an alternating magnetic field strength of 2500 A/m, 5000 A/m, and 10 000 A/m ( $J_{2500}$ ,  $J_{5000}$ ,  $J_{10000}$ ).

### 3. Results and Discussions

#### 3.1. Effect of Process Parameter on Microstructural Evolution

##### 3.1.1. Conventional Annealing Heat Treatment

The effect of the soaking time on the microstructural evolution of the samples subjected to conventional annealing heat treatment is summarized in Table 3, in terms of average grain size and Vickers hardness values. Furthermore, Figure 2 shows the micrographs and the grain size distributions obtained from the statistical analysis.

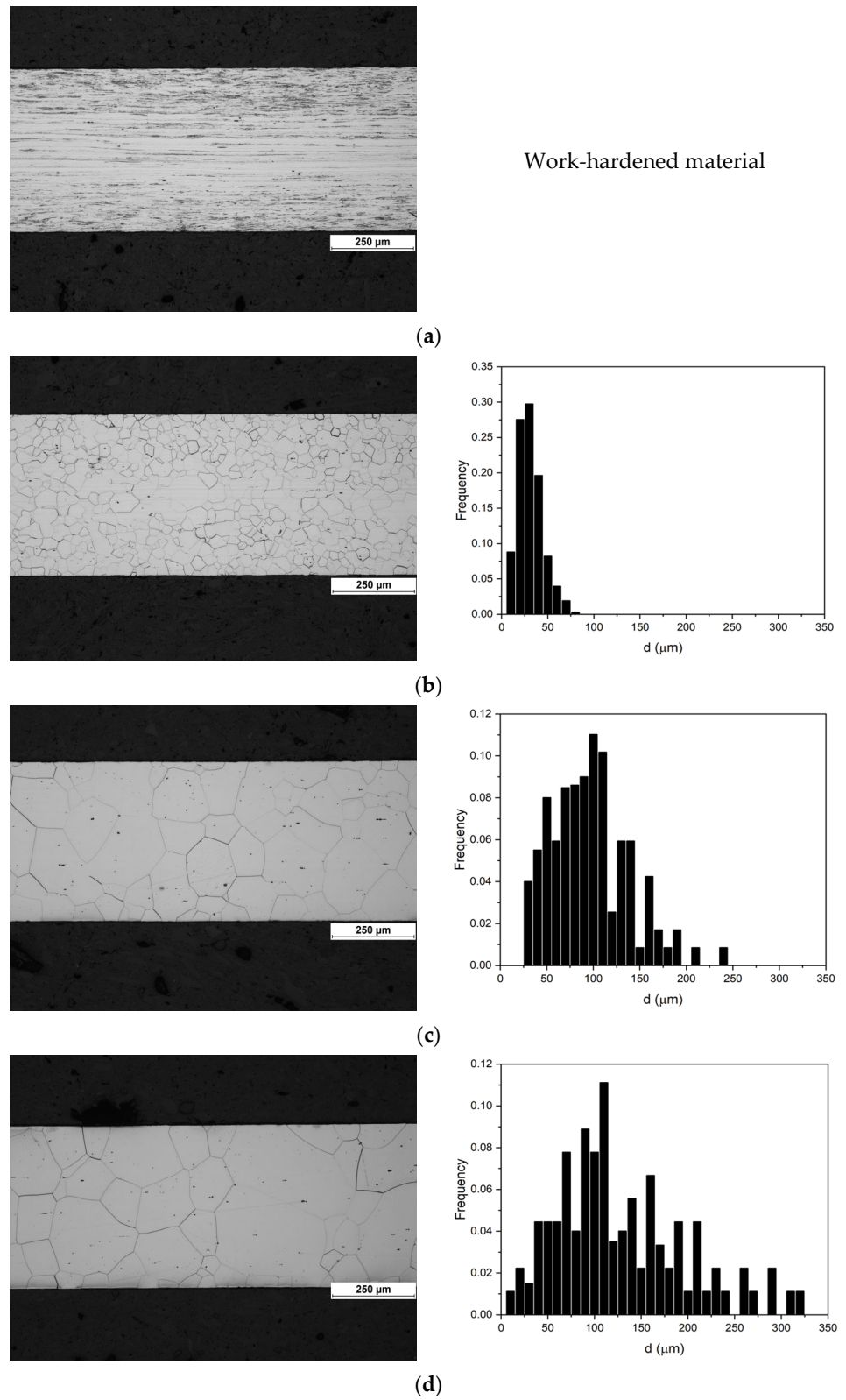


**Figure 2.** Full thickness microstructures and grain size distribution of NGO grade after conventional annealing: (a) heating treatment time 10 s (maximum temperature = 630 °C); (b) heating treatment time 25 s (maximum temperature = 965 °C); (c) heating treatment time 60 s (maximum temperature = 1050 °C); (d) heating treatment time 90 s (maximum temperature = 1050 °C).

Results show that for the sample with a soaking time of 10 s, in which the maximum temperature reached is 630 °C, the material is still strongly work-hardened.

The scenario changes after a soaking time of 25 s and a maximum temperature reached of 965 °C (see Figure 2b) in which, although the temperature is not the target temperature of the desired treatment (1050 °C), the material presents a microstructure with equiaxed grains, an average grain size of  $26.0 \pm 13.0$  mm, and a grain size distribution resembling a log-normal curve typically associated with a recrystallized material. After 60 s and after 90 s of treatment at the target temperature, microstructures undergo grain growth phenomena up to a grain size of  $87.9 \pm 43.6$   $\mu\text{m}$  and  $125.5 \pm 70.4$   $\mu\text{m}$ , respectively. Furthermore, as the heat treatment temperature increases, in addition to a progressive shift towards higher values of the mode of the distribution (average grain size value), a gradual broadening of the distribution is observed. This indicates a heterogeneous dimensional variation characteristic of the various stages of grain growth.

**Table 3.** Average grain size values of conventional annealed samples through intercept method.

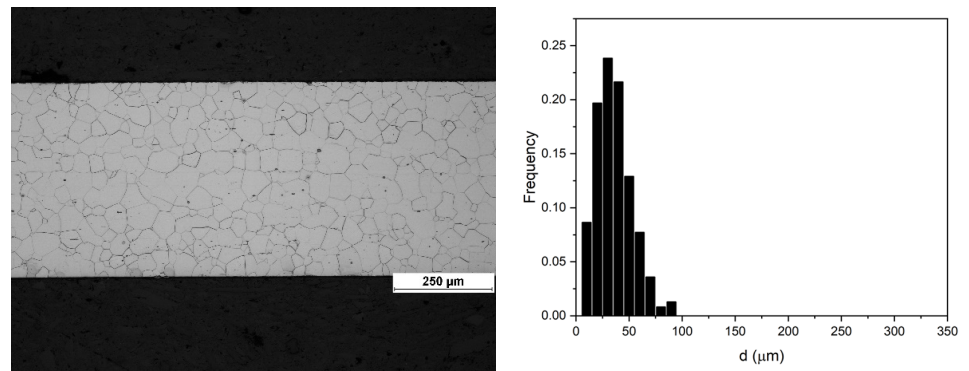
| Soaking Time (s) | Maximum Temperature (°C) | Average Grain Size d ( $\mu\text{m}$ ) | Std. Dev ( $\mu\text{m}$ ) | HV <sub>1</sub> |
|------------------|--------------------------|--|----------------------------|-----------------|
| 10               | 631                      | -                                      | -                          | 279.9 $\pm$ 3.5 |
| 25               | 965                      | 26.0                                   | 13.0                       | 196.4 $\pm$ 2.9 |
| 60               | 1050                     | 87.9                                   | 43.6                       | 193.8 $\pm$ 3.0 |
| 90               | 1050                     | 120.5                                  | 70.4                       | 192.7 $\pm$ 2.7 |

### 3.1.2. Ultra-Fast Heating Treatment

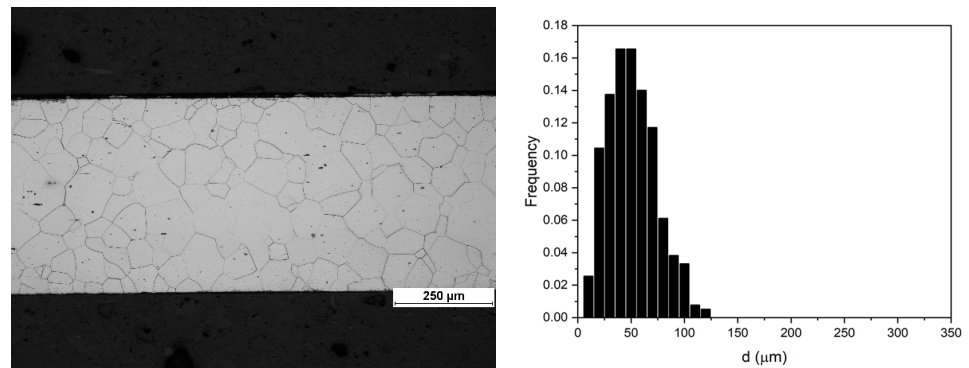
The effect of UFH conditions is summarized in Table 4 in terms of average grain size and Vickers hardness values as a function of different HR and  $T_{\text{peak}}$  (see the treatment conditions in Table 2). Moreover, in Figures 3 and 4, the microstructure evolution and frequency distribution of the grain size are reported, respectively, for the inductor power of 80% and 90%. All samples exhibit a fully recrystallized microstructure and as expected, and as evidenced by the graph shown in Figure 5, an increase in peak temperature results in a linear increase in the average grain size. For each sample, the microstructure appears to be homogeneous over the entire section of the sample, confirming the uniformity of temperature through the sheet thickness during UFH treatment.

**Table 4.** Average grain size and Vickers hardness values of UFH samples.

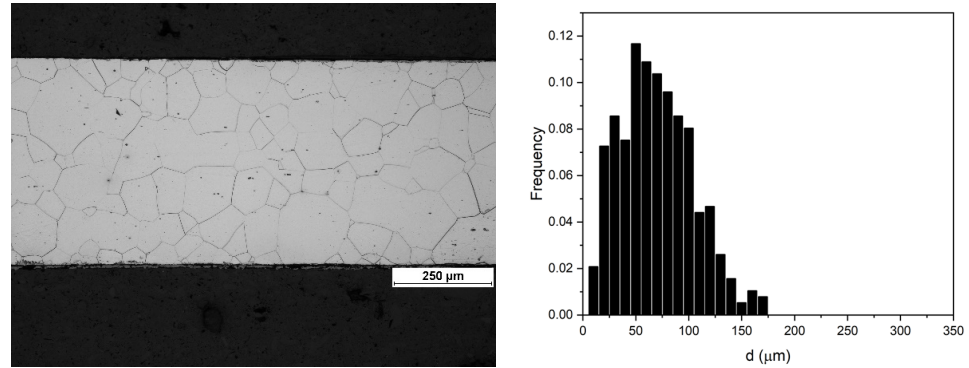
| P% | $T_{\text{peak}}$ (°C) | HR (°C/s) | Average Grain Size d ( $\mu\text{m}$ ) | Std. Dev. ( $\mu\text{m}$ ) | HV <sub>1</sub> |
|----|------------------------|-----------|--|-----------------------------|-----------------|
| 80 | 930                    | 213       | 30.8                                   | 16.5                        | 197.8 $\pm$ 6.3 |
| 80 | 1014                   | 205       | 46.2                                   | 22.6                        | 200.1 $\pm$ 0.8 |
| 80 | 1085                   | 206       | 62.5                                   | 32.3                        | 201.6 $\pm$ 1.3 |
| 80 | 1167                   | 229       | 68.2                                   | 40.4                        | 200.3 $\pm$ 1.2 |
| 90 | 953                    | 267       | 40.8                                   | 22.3                        | 196.6 $\pm$ 2.4 |
| 90 | 1000                   | 254       | 43.7                                   | 22.8                        | 192.6 $\pm$ 2.6 |
| 90 | 1038                   | 264       | 56.2                                   | 30.6                        | 199.2 $\pm$ 5.5 |
| 90 | 1090                   | 265       | 58.0                                   | 32.7                        | 203.1 $\pm$ 5.1 |



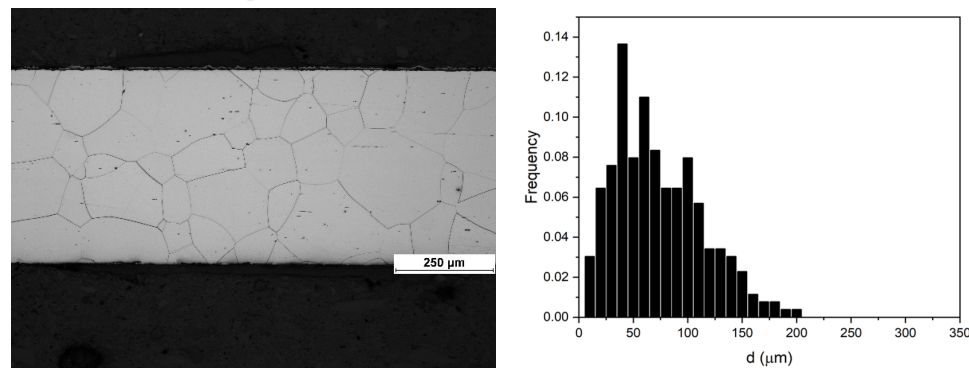
Spec. number: 1, HR = 213 °C/s, T<sub>peak</sub> = 930 °C



Spec. number: 2, HR = 205 °C/s, T<sub>peak</sub> = 1014 °C

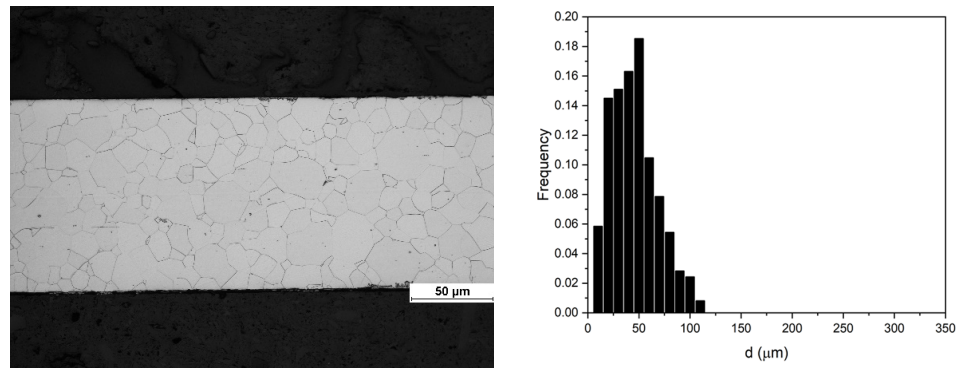


Spec. number: 3, HR = 206 °C/s, T<sub>peak</sub> = 1085 °C

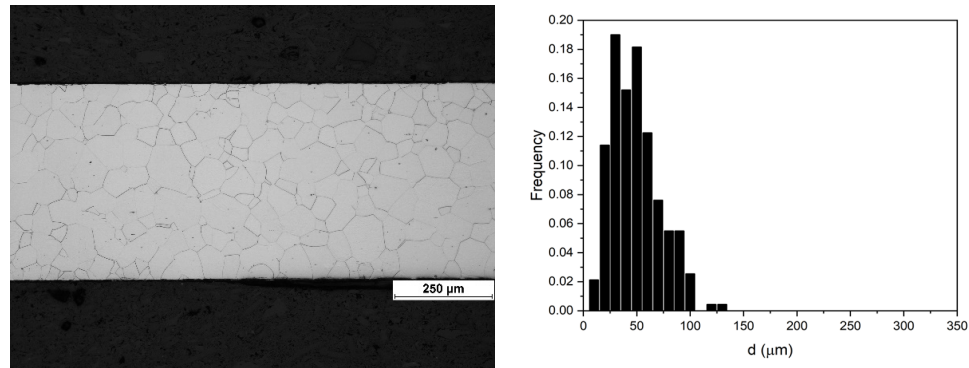


Spec. number: 4, HR = 229 °C/s, T<sub>peak</sub> = 1167 °C

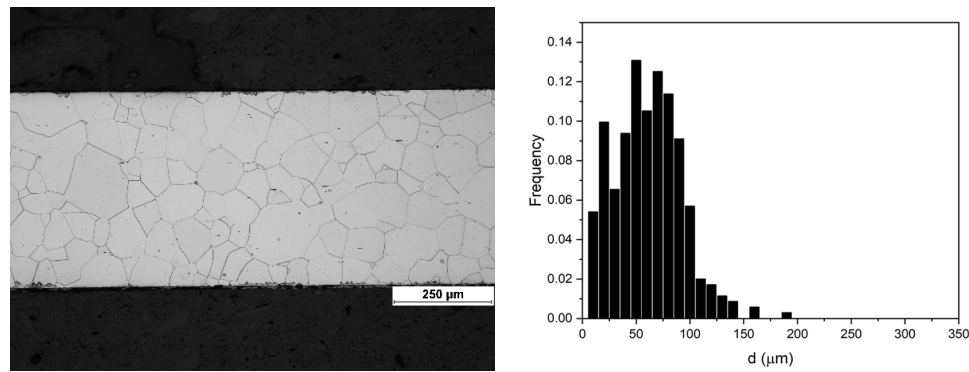
**Figure 3.** Full thickness microstructures and grain size distributions of NGO grade after UFH at P = 80%. Specimen number and annealing treatment conditions according to Table 2.



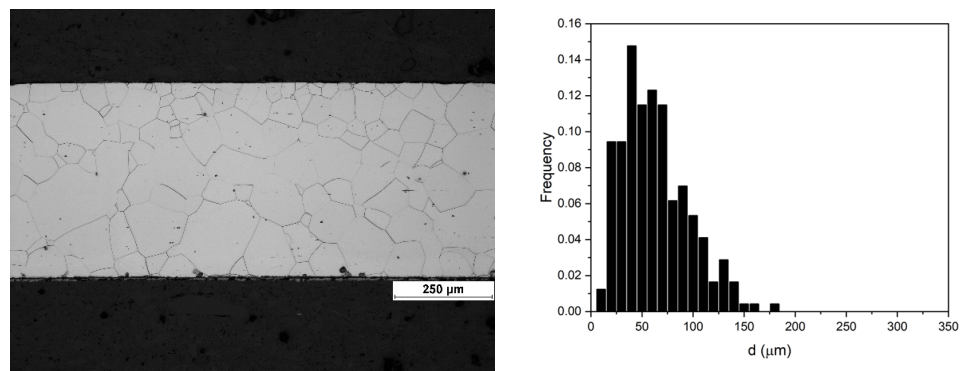
Spec. number: 5, HR = 267 °C/s,  $T_{peak} = 953\text{ °C}$



Spec. number: 6, HR = 254 °C/s,  $T_{peak} = 1000\text{ °C}$

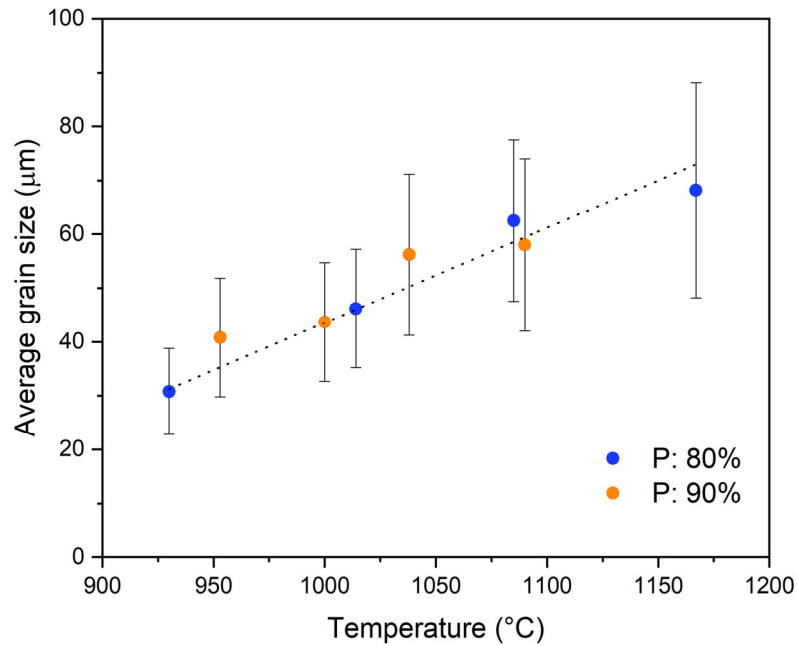


Spec. number: 7, HR = 264 °C/s,  $T_{peak} = 1038\text{ °C}$



Spec. number: 8, HR = 265 °C/s,  $T_{peak} = 1090\text{ °C}$

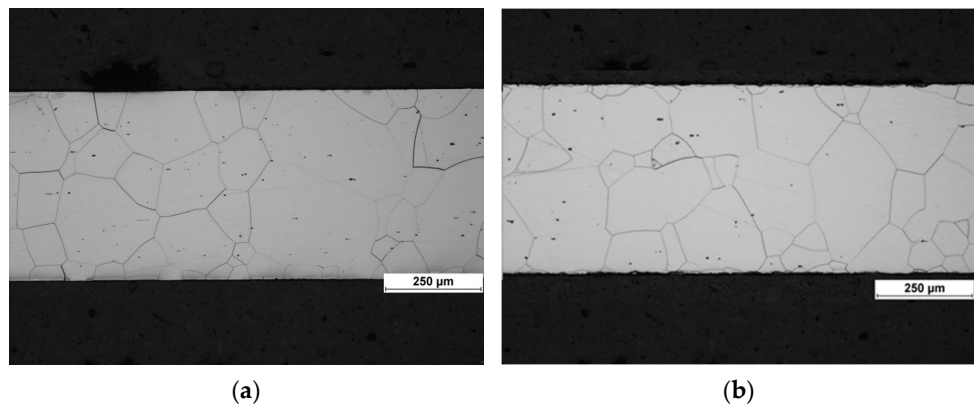
**Figure 4.** Full thickness microstructures and grain size distributions of NGO grade after UFH at P= 90%. Specimen number and annealing treatment conditions according to Table 2.



**Figure 5.** Average values of grain size vs. peak temperature after ultra-fast heating treatment.

Figure 6 compares the microstructures obtained by conventional annealing and UFH ( $P = 90\%$ ,  $HR = 264$  °C/s,  $T_{\text{peak}} = 1038$  °C and  $P = 80\%$ ,  $HR = 206$  °C/s,  $T_{\text{peak}} = 1085$  °C) with that of a conventional industrially produced material of grade M310-50A. The relative average grain sizes and Vickers hardness values are shown in Table 5.

By comparing the material behavior, it is evident that the mean grain size, as well as hardness values for the conventional annealing material and M310-50A material, are very similar. This demonstrates the ability and reliability of the annealing treatment in a laboratory tube furnace in the reproduction of industrially produced microstructures. Instead, the microstructures obtained after UFH are characterized by an average grain size, which is about one half smaller than that obtained by the conventional CA treated. This is a direct consequence of the ultra-fast process, which tends to inhibit the grain growth phenomenon.



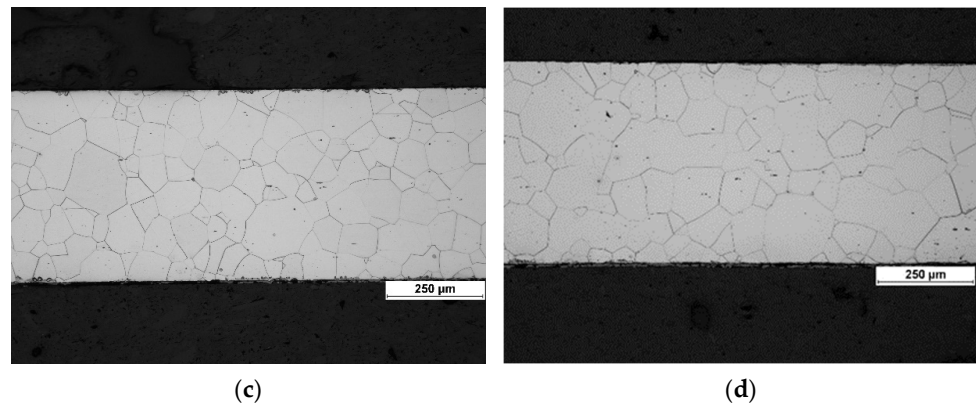


**Figure 6.** Comparison of full thickness microstructures: (a) conventional annealing after 30 s of soaking time at 1050 °C; (b) reference NGO material M310-50A that has undergone industrial annealing process; (c) ultra-fast heating with peak temperature of 1038 °C (HR = 264 °C/s); (d) ultra-fast heating with peak temperature of 1085 °C (HR = 206 °C/s).

**Table 5.** Average grain size comparison between samples that have undergone CA and UFH heat treatments.

| Heat Treatment | Process Conditions                        | Average Grain Size (μm) | HV <sub>1</sub> |
|----------------|---|-------------------------|-----------------|
| CA             | T <sub>peak</sub> : 1050 °C               | 120.5 ± 70.4            | 192.7 ± 2.7     |
| M310-50A       | Industrial reference annealing process    | 104.7 ± 52.7            | 186.3 ± 2.3     |
| UFH            | HR: 206 °C/s, T <sub>peak</sub> : 1038 °C | 56.2 ± 30.6             | 199.2 ± 5.5     |
| UFH            | HR: 264 °C/s, T <sub>peak</sub> : 1085 °C | 62.5 ± 32.3             | 201.6 ± 1.3     |

3.2. Effect of Microstructural Evolution on Mechanical Properties

Tensile test curves are shown in Figure 7. The mechanical properties in terms of Y<sub>s</sub>, R<sub>m</sub>, and A% of the UFH processed material are summarized in Table 6.

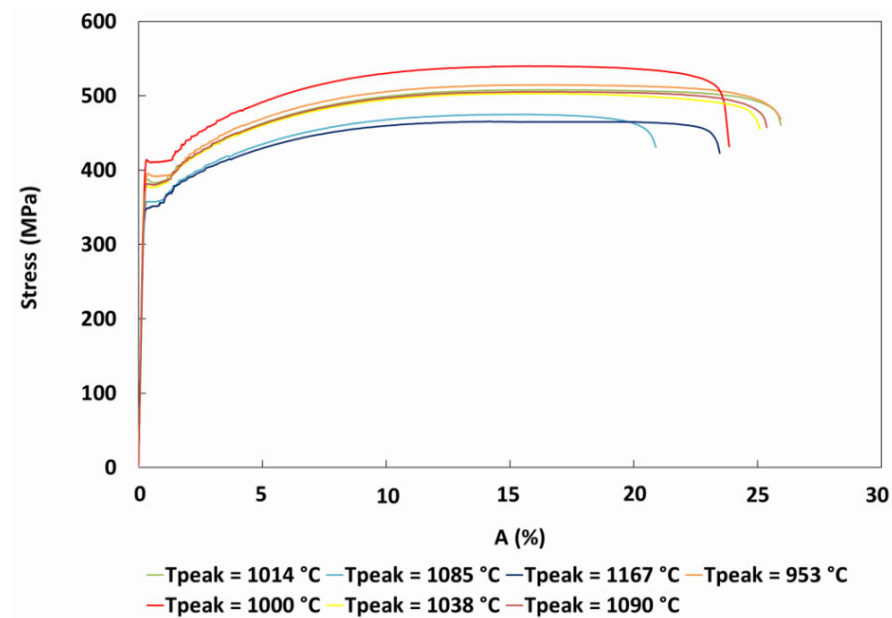


**Figure 7.** Stress–strain curves for materials that have undergone UFH treatment.

**Table 6.** Tensile properties of UFH specimens.

| T <sub>peak</sub> (°C) | Average Grain Size (mm) | R <sub>m</sub> (MPa) | Y <sub>SH</sub> (MPa) | Y <sub>SL</sub> (MPa) | A (%) |
|------------------------|-------------------------|----------------------|-----------------------|-----------------------|-------|
| 1014                   | 46.2                    | 528                  | 401                   | 399                   | 25    |
| 1085                   | 62.5                    | 497                  | 376                   | 374                   | 22    |
| 1167                   | 68.2                    | 473                  | 375                   | 371                   | 23    |
| 953                    | 40.8                    | 527                  | 406                   | 402                   | 26    |
| 1000                   | 43.7                    | 537                  | 413                   | 408                   | 25    |
| 1038                   | 56.2                    | 510                  | 389                   | 386                   | 24    |
| 1090                   | 58.0                    | 508                  | 383                   | 382                   | 24    |

According to the Hall–Petch relationship (Equation (2)), the tensile behavior of a material depends on the average grain size:

$$\sigma_y = \sigma_0 + \frac{k_y}{\sqrt{d}} \tag{2}$$

where  $\sigma_y$  is the yield strength,  $\sigma_0$  is the intrinsic strength of the material (corresponding to a single crystal structure), and  $k_y$  is a constant depending on the alloy. Figure 8 shows the dependence trend between the average grain size and yield strength, showing a linear dependence with  $k_y = 32.7 \text{ MPa mm}^{-1/2}$  and  $\sigma_0 = 245 \text{ MPa}$ .

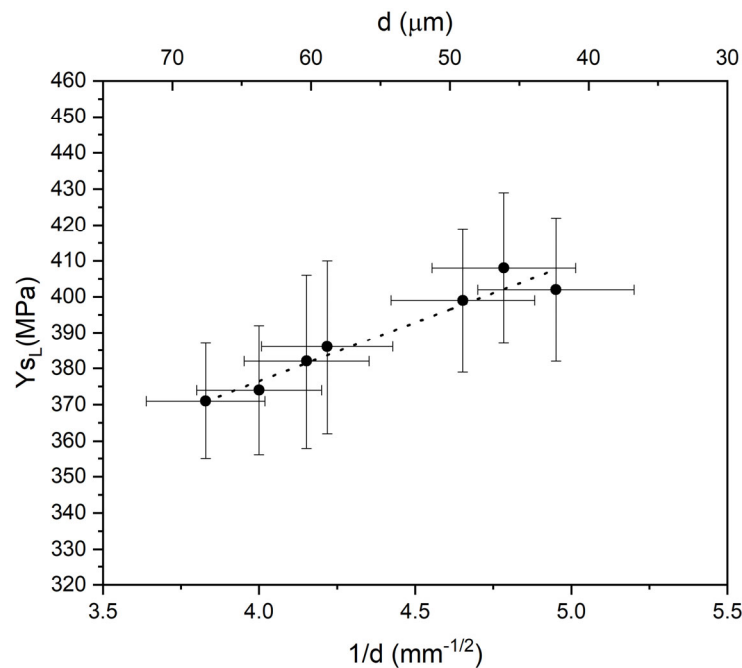


**Figure 8.** Yield strength dependance on grain size.

From the results shown, it follows that the best mechanical resistance corresponds to a T<sub>peak</sub> of 1000 °C. For this sample, the values of R<sub>m</sub>, Y<sub>s</sub>, and A% are highly comparable with those found in the literature for sheets with the same thickness and chemical composition as that investigated in this work [55,72,73]. Therefore, these literature works support the ability to successfully process NGO electrical steels through UFH treatment, providing materials with microstructure and mechanical characteristics comparable to industrial products manufactured with conventional technologies.

### 3.3. Magnetic Measurements Results

The magnetic characterization was carried out in terms of core losses and polarization, obtaining the magnetization curves and the core losses curve.

To evaluate such magnetic properties of the samples processed by UFH, magnetic measurements were performed by SST on both L and T directions. Therefore, the core losses and the polarization values were calculated as the average of the measurements along L and T. Table 7 shows the results for the samples treated with UFH, in which  $P_{10}$  and  $P_{15}$  represent the core losses obtained at  $B = 1.0$  T and  $B = 1.5$  T, respectively. In addition,  $J_{2500}$ ,  $J_{5000}$ , and  $J_{10000}$  represent the polarization values obtained at the magnetic field strength of 2500, 5000, and 10,000 A/m, respectively. The Anisotropy of loss (%) is calculated according to the EN-10106 standard.

**Table 7.** Magnetic properties of UFH specimens obtained by SST measurements.

| P (%)                                  | $T_{\text{peak}}$ (°C) | $P_{10}$ (W/kg) | $P_{15}$ (W/kg) | $J_{2500}$ (T) | $J_{5000}$ (T) | $J_{10000}$ (T) | Anisotropy of Loss (%) |
|--|------------------------|-----------------|-----------------|----------------|----------------|-----------------|------------------------|
| 80                                     | 930                    | 1.52            | 3.32            | 1.57           | 1.65           | 1.76            | 4.2                    |
| 80                                     | 1014                   | 1.54            | 3.36            | 1.56           | 1.65           | 1.76            | 2.0                    |
| 80                                     | 1085                   | 1.47            | 3.26            | 1.55           | 1.63           | 1.75            | 1.6                    |
| 80                                     | 1167                   | 1.36            | 3.10            | 1.54           | 1.63           | 1.75            | 9.6                    |
| 90                                     | 953                    | 1.45            | 3.21            | 1.57           | 1.65           | 1.76            | 3.3                    |
| 90                                     | 1000                   | 1.45            | 3.17            | 1.57           | 1.66           | 1.77            | 3.2                    |
| 90                                     | 1038                   | 1.37            | 3.13            | 1.54           | 1.63           | 1.75            | 10.4                   |
| 90                                     | 1090                   | 1.53            | 3.32            | 1.56           | 1.65           | 1.76            | 3.3                    |
| Industrial reference annealing process |                        | 1.26            | 3.07            | 1.54           | 1.64           | 1.77            | 9.5                    |

The best results in terms of core losses were obtained for the sample treated at the highest peak temperature (1167 °C) with a higher average size ( $68.2 \pm 40.4$  mm), which corresponds to power losses of 3.10 W/kg for a magnetic induction of 1.5 T. This result ( $P_{15} = 3.10$  W/Kg), obtained through the specified UFH treatment, turns out to be the same as that obtained for the sample of reference material industrially produced as non-oriented electrical steel grade M310-50A (EN10106), with the same thickness of 0.50 mm.

In Figure 9, the magnetization curves for UFH samples treated with power induction of 80% and 90% and  $T_{\text{max}}$ , respectively, temperatures of 1085 °C and 1167 °C are reported and compared to the industrially produced M310-50A material.

The magnetization curves for UFH samples treated at 1085 °C and 1167 °C showed similar results with high induction levels. Moreover, such curves appear to be similar to the magnetization curve of the industrial reference material, especially at high induction levels. However, some differences can be observed at the intermediate magnetic field strength.

For the three samples compared, core losses curves show a similar behavior—despite the UFH specimen treated with  $T_{\text{max}} = 1085$  °C, which presents slightly higher core losses (Figure 10). On the other hand, with regards to the UFH sample treated with  $T_{\text{max}} = 1167$  °C, the core losses curve appears to be quite similar to that of the industrial reference M3150-A.

Therefore, the results reported above—obtained from UFH laboratory trials and characterizations—confirm the possibility of obtaining, through ultra-fast heating treatment, NGO grades with magnetic properties comparable to an industrially produced and more expensive non-oriented electrical steel grade.

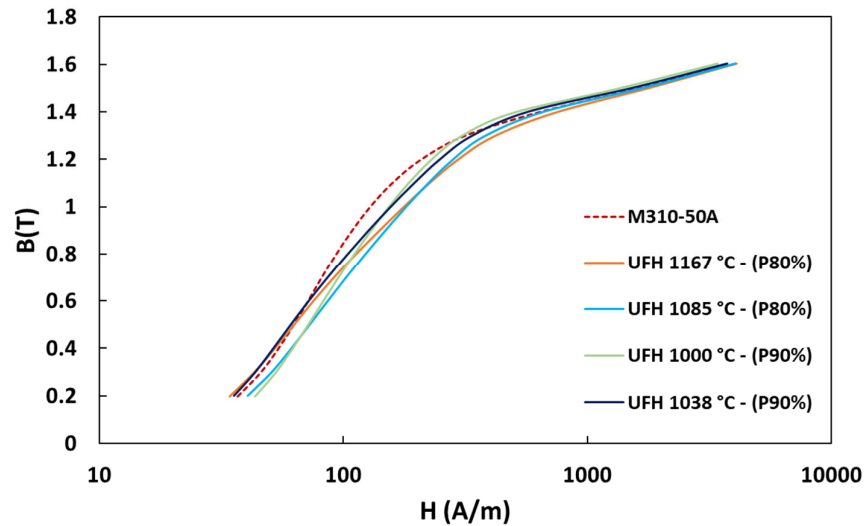


**Figure 9.** Best magnetization curves for UFH samples treated with power induction of 80% and 90%, in comparison with magnetization curve of industrially produced M310-50A material.

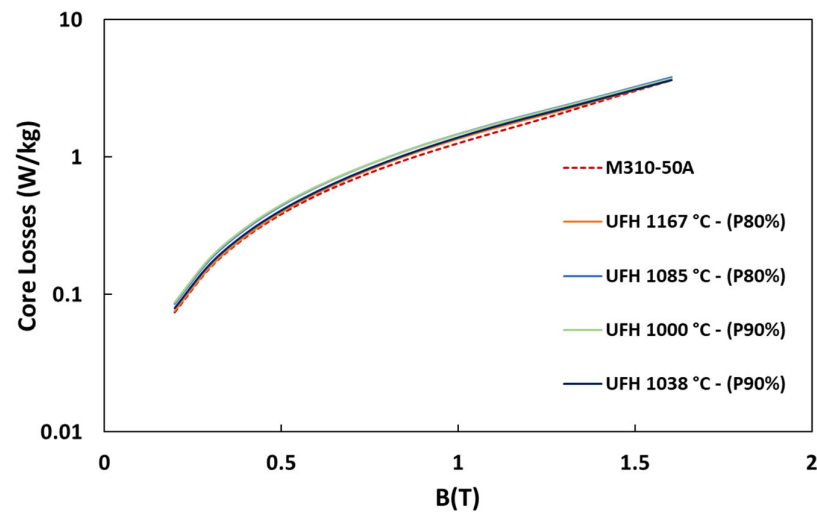


**Figure 10.** Core losses curves for UFH samples treated with power induction of 80% and 90%, in comparison with core losses curve of industrially produced M310-50A material.

#### 4. Conclusions

This paper reports the results of the microstructure characterization, mechanical and magnetic properties of NGO electrical steel (thickness 0.5 mm) which underwent UFH treatment. The results can be summarized as follows.

- The comparison between the microstructures of the samples after conventional annealing, industrial reference annealing, and UFH treatment confirmed that innovative rapid annealing produced a severe grain refinement, with the grain size of UFH samples two times smaller;
- with the UFH cycle, conducted with  $P = 80\%$ ,  $T_{\text{peak}} = 1000\text{ }^{\circ}\text{C}$  and HR:  $254\text{ }^{\circ}\text{C/s}$ , it was possible to achieve tensile properties ( $R_m = 537\text{ MPa}$ ,  $R_{pL} = 408\text{ MPa}$ ,  $R_{pH} = 413\text{ MPa}$ , and  $A: 25\%$ ) comparable with an industrially produced M270-50 steel;
- the magnetic properties evaluated for the same sample that was UFH treated ( $P = 80\%$ ,  $T_{\text{peak}} = 1000\text{ }^{\circ}\text{C}$ , and HR:  $254\text{ }^{\circ}\text{C/s}$ ), showed results comparable with industrially produced NGO steel grade M310-50A.

**Author Contributions:** Conceptualization, L.A. and G.T.; methodology, L.A. and G.T.; formal analysis, M.G., L.L. and G.S.; investigation, M.G. and G.S.; writing-original draft preparation, M.G.; writing-review and editing, all authors; supervision, A.D.S. All authors have read and agreed to the published version of the manuscript.

**Funding:** This research received no external funding.

**Data Availability Statement:** The data presented in this study are available on request from the corresponding authors.

**Conflicts of Interest:** The authors declare no conflicts of interest.

## References

1. Di Schino, A.; Testani, C. Corrosion Behavior and Mechanical Properties of AISI 316 Stainless Steel Clad Q235 Plate. *Metals* **2020**, *10*, 552. <https://doi.org/10.3390/met10040552>.
2. Di Schino, A.; Gaggiotti, M.; Testani, C. Heat Treatment Effect on Microstructure Evolution in a 7% Cr Steel for Forging. *Metals* **2020**, *10*, 808. <https://doi.org/10.3390/met10060808>.
3. Miranda-Pérez, A.F.; Rodríguez-Vargas, B.R.; Calliari, I.; Pezzato, L. Corrosion Resistance of GMAW Duplex Stainless Steels Welds. *Materials* **2023**, *16*, 1847. <https://doi.org/10.3390/ma16051847>.
4. Stornelli, G.; Gaggia, D.; Rallini, M.; Di Schino, A. Heat Treatment Effect on Maraging Steel Manufactured by Laser Powder Bed Fusion Technology: Microstructure and Mechanical Properties. *Acta Metall. Slovaca* **2021**, *27*, 122–126. <https://doi.org/10.36547/ams.27.3.973>.
5. Gomes Landgraf, F.J. Nonoriented Electrical Steels. In *Linking Science and Technology for Global Solutions*; Orlando, FL, USA, 2012.
6. Steiner Petrovic, D. Non-Oriented Electrical Steel Sheets. *Mater. Technol.* **2010**, *44*, 317–325.
7. JFE Steel Corporation (Electrical Steel Business Planning Department). *Electrical Steels for EV Traction Motors in JFE Steel*; JFE Technical Report n° 27; JFE Steel Corporation: Tokyo, Japan, 2022.
8. Fujimura, H.; Hirayama, R.; Wajima, K.; Yamazaki, S. *Nippon Steel Technical Report No. 122*; Nippon Steel: Tokyo, Japan, 2019.
9. Enokizono, M.; Suzuki, T.; Sievert, J.D.; Xu, J. Rotational power loss of silicon steel sheet. *IEEE Trans. Magn.* **1990**, *26*, 2562–2564.
10. Senda, K.; Uesaka, M.; Yoshizaki, S.; Oda, Y. Electrical Steels and Their Evaluation for Automobile Motors. *World Electr. Veh. J.* **2019**, *10*, 31.
11. Faba, A.; Riganti Fulginei, F.; Quondam Antonio, S.; Stornelli, G.; Di Schino, A.; Cardelli, E. Hysteresis modelling in additively manufacturing FeSi magnetic components for electrical machines and drives. *IEEE Trans. Ind. Electron.* **2023**, *26*, 2562–2564. <https://doi.org/10.1109/TIE.2023.3269483>.
12. Stornelli, G.; Faba, A.; Di Schino, A.; Folgarait, P.; Ridolfi, M.; Cardelli, E.; Montanari, R. Properties of additively manufactured electric steel powder cores with increased Si content. *Materials* **2021**, *14*, 1489.
13. Rodríguez-Vargas, B.R.; Stornelli, G.; Folgarait, P.; Ridolfi, M.R.; Miranda Pérez, A.F.; Di Schino, A. Recent Advances in Additive Manufacturing of Soft Magnetic Materials: A Review. *Materials* **2023**, *16*, 5610.
14. Di Schino, A.; Stornelli, G. Additive manufacturing: A new concept for end users. The case of magnetic materials. *Acta Metall. Slovaca* **2022**, *28*, 208–211.
15. Sidor, J.J.; Verbeken, V.; Gomes, G.; Schneider, S.; Rodríguez Calvillo, P.; Kestens, L.A.I. Through process texture evolution and magnetic properties of high Si non-oriented electrical steels. *Mater. Charact.* **2012**, *71*, 49–57.
16. Hawezy, H. The influence of silicon content on physical properties of non-oriented silicon steel. *Mater. Sci. Technol.* **2017**, *33*, 1560–1569.
17. Lee, K.M.; Park, P.; Huh, H.; Kim, K.; Engler, E. Effect of texture and grain size on magnetic flux density and core loss in non-oriented electrical steel containing 3.15% Si. *J. Magn. Magn. Mater.* **2014**, *354*, 324–332.
18. Ren, Q.; Hu, Z.; Cheng, L.; Zhang, L. Effect of rare earth elements on magnetic properties of non-oriented electrical steels. *J. Magn. Magn. Mater.* **2022**, *560*, 169624.
19. Mehdi, M.; He, Y.; Hilinski, E.J.; Kar, N.C.; Edrissy, A. Non-oriented electrical steel with core losses comparable to grain-oriented electrical steel. *J. Magn. Magn. Mater.* **2019**, *491*, 165597.
20. Fischer, O.; Schneider, J. Influence of deformation process on the improvement of non-oriented electrical steel. *J. Magn. Magn. Mater.* **2003**, *254–255*, 302–306.
21. Ferreira-De Dafê, S.S.; Da Costa-Paolinelli, S.; Cota, A.B. Influence of thermomechanical processing on shear bands formation and magnetic properties of a 3% Si non-oriented electrical steel. *J. Magn. Magn. Mater.* **2011**, *323*, 3234–3238.
22. He, Q.; Zhu, C.; Liu, Y.; Wen Yan, E.; Wan, W.; Li, L. Effect of annealing temperature on the properties of phosphorus micro-alloyed non-oriented electrical steels. *J. Mater. Res. Technol.* **2023**, *23*, 4454–4465.
23. Stocker, A.; Prah, U.; Kawalla, R. Impact of hot rolling condition on microstructure, texture, and magnetic properties of ferritic Fe-2.4wt.% Si non-oriented electrical steel. In *Proceedings of the International Conference on Magnetism and Metallurgy, Milan, Italy, 13–15 June 2022*.
24. An, L.; Wang, Y.; Song, H.; Wang, G.; Liu, H. Improving magnetic properties of non-oriented electrical steels by controlling grain size prior to cold rolling. *J. Magn. Magn. Mater.* **2019**, *491*, 165636.

25. Sidor, Y.; Kovac, F. Microstructural aspects of grain growth kinetics in non-oriented electrical steels. *Mater. Charact.* **2005**, *55*, 1–11.
26. Shimanaka, H.; Ito, Y.; Matsumura, K.; Fukuda, B. Recent development of non-oriented electrical steel sheets. *J. Magn. Magn. Mater.* **1982**, *26*, 57–64.
27. Liu, H.; Li, H.; Wang, H.; Liu, Y.; Gao, F.; An, L.; Zhao, S.; Liu, Z.; Wang, G. Effects of initial microstructure and texture on microstructure, texture evolution and magnetic properties of non-oriented electrical steel. *J. Magn. Magn. Mater.* **2016**, *406*, 149–158.
28. Jiao, H.T.; Xu, Y.B.; Zhao, L.Z.; Misra, R.D.K.; Tang, Y.C.; Zhao, M.J.; Liu, D.J.; Hu, Y. Microstructural evolution and magnetic properties in strip cast non-oriented silicon steel produced by warm rolling. *Mater. Charact.* **2019**, *156*, 109876.
29. Ferreira Rodrigues, M.; De Cunha, M.A.; Da Costa Paolinelli, S.; Cota, A.B. Texture and magnetic properties improvement of a 3% Si non-oriented electrical steel by Sb addition. *J. Magn. Magn. Mater.* **2013**, *331*, 24–27.
30. Stornelli, G.; Gaggiotti, M.; Mancini, S.; Napoli, G.; Rocchi, C.; Tirasso, C.; Di Schino, A. Recrystallization and grain growth of super austenitic stainless steel AISI 904L: A multivariate regression approach. *Metals* **2022**, *12*, 200.
31. Di Schino, A.; Kenny, J.M.; Salvatori, I.; Abbruzzese, G. Modelling the primary recrystallization and grain growth in a low nickel austenitic stainless steel. *J. Mat. Sci.* **2001**, *36*, 593–600.
32. Stornelli, G.; Di Schino, A.; Mancini, S.; Montanari, R.; Testani, C.; Varone, A. Grain refinement and improved mechanical properties of EUROFER97 by thermo-mechanical treatments. *Appl. Sci.* **2021**, *11*, 10598.
33. Franke, A.; Schneider, J.; Stocker, A.; Kawalla, R. Warm Rolling of Ferritic Nonoriented FeSi Steels. In Proceedings of the International Conference on Magnetism and Metallurgy, Milan, Italy, 13–15 June 2022.
34. Cong, J.; Guo, F.; Qiao, J.; Qiu, S.; Wang, H. Optimum Magnetic Properties of Non-Oriented Electrical Steel Produced by Compat Strip Production Process. *Metals* **2022**, *12*, 64.
35. Gutierrez-Castaneda, E.J.; Salinas-Rodriguez, A. Effect of annealing prior to cold rolling on magnetic and mechanical properties of low carbon non-oriented electrical steels. *J. Magn. Magn. Mater.* **2011**, *323*, 2524–2530.
36. Qiao, J.; Liu, L.; Guo, F.; Xiang, L.; Qiu, S.; Wang, H. Effect of hot band annealing on inclusions, texture, and magnetic properties of 2.97%Si-0.57%Al non-oriented silicon steel. *Ironmak. Steelmak.* **2018**, *47*, 22–30.
37. Xu, Y.B.; Zhang, Y.X.; Wang, Y.; Li, C.G.; Cao, G.M.; Liu, Z.Y.; Wang, G.D. Evolution of cube texture in strip-cast non-oriented silicon steels. *Scr. Mater.* **2014**, *87*, 17–20.
38. Liu, H.T.; Li, H.Z.; Li, H.L.; Gao, F.; Liu, G.H.; Luo, Z.H.; Zhang, F.Q.; Chen, S.L.; Cao, G.M.; Liu, Z.Y.; et al. Effects of rolling temperature on microstructure, texture, formability, and magnetic properties in strip casting Fe-6.5 wt% Si non-oriented electrical steel. *J. Magn. Magn. Mater.* **2015**, *391*, 65–74.
39. Lu, Y.; Zu, G.; Luo, L.; Wang, Y.; Gao, L.; Yuan, L.; Ran, X.; Zhang, X. Investigation of microstructure and properties of strip-cast 4.5 wt% Si non-oriented electrical steel by different rolling processes. *J. Magn. Magn. Mater.* **2020**, *497*, 165975.
40. Bian, X.; Zeng, Y.; Nan, D.; Wu, M. The effect of copper precipitates on the recrystallization textures and magnetic properties of non-oriented electrical steels. *J. Alloys Compd.* **2014**, *588*, 108–113.
41. Jenkins, K.; Lindemno, M. Precipitates in electrical steels. *J. Magn. Magn. Mater.* **2008**, *320*, 2423–2429.
42. Schulte, M.; Steentjes, S.; Leuning, N.; Bleck, W.; Hameyer, K. Effect of manganese in high silicon alloyed non-oriented electrical steel sheets. *J. Magn. Magn. Mater.* **2019**, *477*, 372–381.
43. Du, Y.; O'Malley, R.J.; Buchely, M.F.; Kelly, P. Effect of rolling process on magnetic properties of Fe-3.3 wt% Si non-oriented electrical steel. *Appl. Phys. A* **2022**, *128*, 765.
44. Kawamata, R.; Kubota, T.; Yamada, K. The effect of cold rolling parameters on the recrystallization texture of non-oriented electrical steel. *J. Mater. Eng. Perform.* **1997**, *6*, 701–709.
45. Huang, B.Y.; Yamamoto, K.; Kaido, C.; Yamashiro, Y. Effect of cold-rolling on magnetic properties of non-oriented silicon steel sheets (Part II). *J. Magn. Magn. Mater.* **2000**, *209*, 197–200.
46. Ghosh, P.; Chromik, R.R.; Knight, A.M.; Wakade, S.G. Effect of metallurgical factors on the bulk magnetic properties of non-oriented electrical steels. *J. Magn. Magn. Mater.* **2014**, *356*, 42–51.
47. Arato, P.; Boc, I.; Grof, T. Effect of composition on the loss of non-oriented medium silicon electrical steels. *J. Magn. Magn. Mater.* **1984**, *41*, 53–55.
48. Hong, J.; Choi, H.; Lee, S.; Kim, J.K.; Koo, Y. Effect of Al content on magnetic properties of Fe-Al non-oriented electrical. *J. Magn. Magn. Mater.* **2017**, *439*, 343–348.
49. Mehdi, M.; He, Y.; Hilinski, E.J.; Kestens, L.A.I.; Edrissy, A. The evolution of cube ( $\{001\}<100>$ ) texture in non-oriented electrical steel. *Acta Mater.* **2020**, *185*, 540–554.
50. Jiqo, H.; Xu, Y.; Zhao, L.; Misra, R.D.K.; Tang, Y.; Liu, D.; Hu, Y.; Zhao, M.; Shen, M. Texture evolution in twin-roll strip cast non-oriented electrical steel with strong Cube and Goss texture. *Acta Mater.* **2020**, *199*, 311–325.
51. Shiozaki, M.; Kurosaki, Y. Anisotropy of magnetic properties in non-oriented electrical steel sheets. *Textures Microstruct.* **1989**, *11*, 159–170.
52. Sonboli, A.; Reza Toroghinejad, M.; Edris, H.; Szpunar, J.A. Effect of deformation route and intermediate annealing on magnetic anisotropy and magnetic properties of a 1 wt% Si non-oriented electrical steel. *J. Magn. Magn. Mater.* **2015**, *385*, 331–338.
53. Chwastek, K. Anisotropic properties of non-oriented steel sheets. *IET Electr. Power Appl.* **2013**, *7*, 575–579.

54. Tanaka, I.; Yashiki, H. Magnetic and Mechanical Properties of Newly Developed High-Strength Nonoriented Electrical Steel. *IEEE Trans. Magn.* **2010**, *46*, 290–293.
55. Leuning, N.; Schauerte, B.; Hameyer, K. Interrelation of mechanical properties and magneto-mechanical coupling of non-oriented electrical steel. *J. Magn. Magn. Mater.* **2023**, *567*, 170322.
56. Dai, J.; Meng, Q.; Zheng, H. High-strength dual-phase steel produced through fast-heating annealing method. *Results Mater.* **2020**, *5*, 100069.
57. Gaggiotti, M.; Albini, L.; Di Nunzio, P.E.; Di Schino, A.; Stornelli, G. Ultrafast heating heat treatment effect on microstructure and properties of steels. *Metals* **2022**, *12*, 1313.
58. Matlock, K.D.; Kang, S.; De Moor, E.; Speer, G.J. Applications of rapid thermal processing to advanced high strength sheet steel developments. *Mater. Charact.* **2020**, *166*, 110397.
59. Wen, P.; Hu, B.; Han, J.; Luo, H. A strong and ductile medium Mn steel manufactured via ultrafast heating process. *J. Mater. Sci. Technol.* **2022**, *97*, 54–68.
60. Jian, W.; Jun, L.; Xin-feng, W.; Jian-jun, T.; Cai-hong, Z.; Shen-gen, Z. Effect of heating rate on microstructure evolution and magnetic properties of cold rolled non-oriented electrical steel. *J. Iron Steel Res. Int.* **2010**, *17*, 54–61.
61. Fang, F.; Xu, Y.; Zhang, Y.X.; Wang, Y.; Lu, X.; Misra, R.D.; Wang, G.D. Evolution of recrystallization microstructure and texture during rapid annealing in strip-cast non-oriented electrical steels. *J. Magn. Magn. Mater.* **2015**, *381*, 433–439.
62. Wang, J.; Li, J.; Mi, X.; Zhang, S.; Volinsky, A.A. Rapid annealing effects on microstructure, texture, and magnetic properties of non-oriented electrical steel. *Met. Mater. Int.* **2012**, *18*, 531–537.
63. Cheng, L.; Yang, P.; Fang, Y.; Mao, W. Preparation of non-oriented silicon steel with high magnetic induction using columnar grains. *J. Magn. Magn. Mater.* **2012**, *324*, 4068–4072.
64. Stornelli, G.; Albini, L.; Tiracorrendo, G.; Rodriguez Vargas, B.R.; Di Schino, A. Effect of ultra-fast heating on AISI 441 ferritic stainless steel. *Acta Metall. Slovaca* **2023**, *29*, 22–25.
65. Rodriguez-Vargas, B.R.; Albini, L.; Tiracorrendo, G.; Massi, R.; Stornelli, G.; Di Schino, A. Effect of ultrafast heating on AISI 304 austenitic stainless steel. *Acta Metall. Slovaca* **2023**, *29*, 104–107. <https://doi.org/10.36547/ams.29.2.1833>.
66. Vercruyssen, F.; Castro Cerda, F.M.; Verleysen, P.; Petrov, R.H. Behavior of ultrafast annealed advanced high strength steels under static and dynamic conditions. *Mater. Sci. Eng. A* **2020**, *780*, 139168.
67. Hernandez-Duran, E.I.; Corallo, L.; Ros-Yanez, T.; Castro-Cerda, F.M.; Petrov, R.H. Influence of Mo–Nb–Ti additions and peak annealing temperature on the microstructure and mechanical properties of low alloy steels after ultrafast heating process. *Mater. Sci. Eng. A* **2021**, *808*, 140928.
68. Tan, X.; Lu, W.; Rao, X. Effect of ultra-fast heating on microstructure and mechanical properties of cold-rolled low-carbon low-alloy Q&P steels with different austenitizing temperature. *Mater. Charact.* **2022**, *191*, 112086.
69. Valdes-Tabernerero, M.A.; Monclus, M.A.; Sabirov, I.; Molina-Aldareguia, J.M.; Petrov, R.H.; Wang, J.; Timokhina, I. The effect of ultrafast heating rate on the elemental distribution between phases in a low carbon steel. *Eur. J. Mater.* **2022**, *2*, 171–185.
70. Yonemura, M.; Nishibata, H.; Fujimura, R.; Ooura, N.; Hata, K.; Fujiwara, K.; Kawano, K.; Yamaguchi, I.; Terai, T.; Inubushi, Y.; et al. Fine microstructure formation in steel under ultrafast heating and cooling. *Sci. Rep.* **2022**, *12*, 2237.
71. Valdes-Tabernerero, M.A.; Kumar, A.; Petrov, R.H.; Monclus, M.A.; Molina-Aldareguia, J.M.; Sabirov, I. The sensitivity of the microstructure and properties to the peak temperature in an ultrafast heat treated low carbon-steel. *Mater. Sci. Eng. A* **2020**, *776*, 138999.
72. Leuning, N.; Steentjes, S.; Schulte, M.; Bleck, W.; Hameyer, K. Effect of elastic and plastic tensile mechanical loading on the magnetic properties of NGO electrical steel. *J. Magn. Magn. Mater.* **2016**, *417*, 42–48.
73. Stocker, A.; Weiner, M.; Korpala, G.; Prah, U.; Wei, X.; Lohmar, J.; Hirt, G.; Heller, M.; Korte-Kerzel, S.; Bohm, L.; et al. Integrated process simulation of non-oriented electrical steel. *Materials* **2021**, *14*, 6659.

**Disclaimer/Publisher's Note:** The statements, opinions and data contained in all publications are solely those of the individual author(s) and contributor(s) and not of MDPI and/or the editor(s). MDPI and/or the editor(s) disclaim responsibility for any injury to people or property resulting from any ideas, methods, instructions or products referred to in the content.